

## Plane-rotator lattice gas in an external orienting field

S. Romano\*

*Instituto Nazionale per la Fisica della Materia e Dipartimento di Fisica "A. Volta," Università di Pavia,  
via Agostino Bassi 6, I-27100 Pavia, Italy*

R. O. Sokolovskii†

*Institute for Condensed Matter Physics, Svientsitskii 1, Lviv 79011, Ukraine  
(Received 31 August 1999; revised manuscript received 27 December 1999)*

We consider a lattice gas of particles that carry a two-component classical spin (i.e., a two-component unit vector). The pair interaction, restricted to nearest neighbors, implicitly includes hard-core repulsion, since each site can host one particle at most, and also contains ferromagnetic interaction between spins as well as nonmagnetic attraction between particles. We study thermodynamic properties and phase diagrams of the model by means of mean-field and two-site cluster approximations, and also by grand-canonical Monte Carlo simulations carried out for one value of the chemical potential; these aim at a quantitative check of the named approximations, as well as a more detailed description. Both mean-field and two-site cluster approximations were found to provide a qualitatively correct description for the thermodynamics of the model with nearest-neighbor interactions, and the predictions of the two-site cluster approximation were in satisfactory quantitative agreement with simulation results. According to both mean-field and two-site cluster treatments, the temperature-density phase diagrams of the model at zero external field are similar to those of the Ising lattice gas, but the effect of external field is quite different. In particular, at zero nonmagnetic attraction the field effect on the gas-liquid critical temperature becomes nonmonotonic. Having compared the field effects in the Ising, plane-rotator, and Heisenberg spin fluids, we conclude that the ability of the external field to decrease the gas-liquid critical temperature weakens with increasing number of spin components.

### I. INTRODUCTION AND POTENTIAL MODEL

Statistical mechanical models consisting of quantum mechanical spin operators, or of "classical spins" (i.e., unit vectors) associated with a lattice have been extensively studied in the literature, especially in their saturated-lattice (SL) version, where each site is occupied by a particle; lattice-gas (LG) extensions of these models can also be defined, where each lattice site hosts one particle at most, and site occupation is also controlled by the chemical potential  $\mu$ .

SL spin models are first defined here: we consider a classical system, consisting of  $n$ -component unit vectors  $\mathbf{u}_k$  (usually  $n=2,3$ ), associated with a  $d$ -dimensional lattice  $Z^d$ , and let  $u_k^\alpha$  denote Cartesian spin components; particle orientations are parametrized by usual polar angles  $\{\varphi_j\}$  ( $n=2$ ) or  $\{(\varphi_j, \theta_j)\}$  ( $n=3$ ); moreover, for each lattice site  $k$ , let  $q_k$  denote site parity, i.e.,  $q_k = \pm 1$  depending on the sum of its  $d$  coordinates being even or odd. Let  $z=2d$  denote the first coordination number of the lattice.

The interaction potential is assumed to be translationally invariant, ferromagnetic, and, in general, anisotropic in spin space

$$W_{jk} = -\epsilon \left[ a u_j^n u_k^n + b \sum_{\alpha < n} u_j^\alpha u_k^\alpha \right]; \quad \epsilon > 0, \quad a \geq 0, \quad b \geq 0, \quad \max(a, b) = 1, \quad (1.1)$$

and the Hamiltonian is

$$\Lambda = \sum_{j < k} W_{jk} = \frac{1}{2} \sum_{j, k} W_{jk}. \quad (1.2)$$

Here and in the following,  $\sum_{j, k}$  is restricted to nearest neighbors, the notation  $\sum_{j < k}$  means that each distinct pair is counted once, and  $\epsilon$  is a positive quantity setting energy and temperature scales.

When  $n=2$ , the pair potential in Eq. (1.1) can be generalized to

$$W_{jk, m} = -\epsilon [ a \cos(m\varphi_j) \cos(m\varphi_k) + b \sin(m\varphi_j) \sin(m\varphi_k) ], \quad (1.3)$$

where  $m$  is an arbitrary positive integer; one can easily check<sup>1,2</sup> that, for any given values of  $a$  and  $b$ , the partition function is independent of  $m$ , and that various structural properties can be defined in a way independent of  $m$ , and actually calculated using any convenient value of it. The choice  $m=1$  defines the ferromagnetic interpretation, whereas  $m=2$  can be interpreted as defining a nematogenic lattice model where three-component spins are constrained to lie in a plane by a suitable external field.<sup>3,4</sup>

Isotropic  $O(n)$ -symmetric models correspond to  $a=b$ ,  $W_{jk} = -\epsilon \mathbf{u}_j \cdot \mathbf{u}_k$  and are referred to as plane rotators ( $n=2$ ) or classical Heisenberg model ( $n=3$ ); the extremely anisotropic and  $O(2)$ -symmetric  $xy$  model is defined by  $n=3$ ,  $a=0$ ; other extremely anisotropic and  $O(1)$ -symmetric models (hereafter called A2 and A3) correspond to  $n=2$ ,  $b=0$  and  $n=3$ ,  $b=0$ , respectively. When  $d=1$ , or when  $d=2$  and the interaction is isotropic in spin space, the potential models produce orientational disorder and no ordering

transition at finite temperature;<sup>5,6</sup> when  $d=2$ , and the interaction is anisotropic in spin space, with  $a>b\geq 0$ , the model supports a ferromagnetic ordering transition at finite temperature (*FMT* for short); when  $d=3$ , isotropic interactions and  $xy$  model suffice to produce a *FMT*.<sup>5,6</sup>

Lattice-gas extensions of the continuous-spin potential models considered here are defined by Hamiltonians

$$\Lambda = \sum_{j<k} (\nu_j \nu_k) (-\lambda + W_{jk}) - \mu N, \quad N = \sum_j \nu_j, \quad (1.4)$$

where  $\nu_j=0,1$  denotes occupation numbers; notice that  $\lambda > 0$  reinforces the orientation-dependent term, whereas  $\lambda < 0$  opposes it, and that a finite value of  $\lambda$  only becomes immaterial in the SL limit  $\mu \rightarrow +\infty$ .

Some rigorous results entailing existence or absence of an ordering transition are also known for LG models with continuous spins.<sup>7-10</sup> On the one hand, it has been proven that, when  $W_{jk}$  produces orientational disorder at all finite temperatures in the SL version, this also happens for its LG extensions. On the other hand, in some cases where  $W_{jk}$  produces a *FMT* in the SL version (e.g., isotropic interactions in three dimensions, or *A2* and *A3* models in two dimensions), this has also been proven to take place for  $\lambda \geq 0$  and sufficiently large  $\mu > 0$ ; results entailing existence or absence of a *FMT* are also known for long-range interactions and  $d=1,2$ .

More recently, it has been proven that, for appropriate ranges of values of  $\lambda < 0$  and  $\mu > 0$ , the ground state possesses staggered positional order, where sites of a certain parity are preferentially occupied, and that this survives up to some finite temperature.<sup>11</sup>

Spin LGs allow to describe various complex systems. In this paper we consider various spin LGs as models of anisotropic fluids,<sup>12</sup> but let us note that they can be considered in many other frameworks, such as segregation in magnetic alloys<sup>13,14</sup> and absorption phenomena.<sup>15-20</sup>

The properties of anisotropic fluids, (for example, of liquid crystals and ferrofluids) are determined by the interplay of spatial and orientational degrees of freedom. In particular, an external magnetic field can initiate the spatial ordering by aligning the spins and, thus, influence the structure of the fluid. This allows to control properties of the anisotropic fluids dynamically. This possibility has inspired several studies of effects of the external magnetic field in the fluids with Ising<sup>12,13,21</sup> and Heisenberg<sup>22-24</sup> spins. Let us note that both the Ising and Heisenberg LGs can be described by the generic Hamiltonian

$$\begin{aligned} \Lambda = & - \sum_{j<k} (\nu_j \nu_k) (\lambda + \epsilon \mathbf{u}_j \cdot \mathbf{u}_k) - \mathbf{h} \cdot \sum_j \nu_j \mathbf{u}_j - \mu \sum_j \nu_j \\ & + \sum_j \nu_j [(\kappa^y u_j^y)^2 + (\kappa^z u_j^z)^2]; \end{aligned} \quad (1.5)$$

here  $\mathbf{u}_j = (u_j^x, u_j^y, u_j^z)$  is a three-dimensional unit vector, and  $\mathbf{h}$  is the external (orienting) magnetic field. The ‘‘disorienting’’ fields  $\kappa^y, \kappa^z$  introduce easy plane anisotropies and allow us to incorporate in Eq. (1.5) the Heisenberg ( $\kappa^y = \kappa^z = 0$ ), plane rotator ( $\kappa^y = 0, \kappa^z = \infty$ ) and Ising ( $\kappa^y = \kappa^z = \infty$ ) lattice gases as special cases.

In the absence of the external magnetic field ( $\mathbf{h}=0$ ) the phase diagrams of Ising<sup>12</sup> and classical Heisenberg<sup>22</sup> fluids appear to be rather similar: at low temperatures, both fluids become ferromagnetic as soon as the density exceeds certain ( $T$ -dependent) threshold, and the resulting phase transition is of the second order. At even lower temperatures this transition becomes coupled<sup>25</sup> with the gas-liquid segregation and is of the first order.<sup>26,27</sup> The ordering external field  $\mathbf{h}$  removes the magnetic order-disorder transition; nevertheless the first order transitions between magnetically ordered phases of different densities survive. And here qualitative differences appear, i.e., the effect of  $\mathbf{h}$  on the transition depends on spin model: at  $\lambda=0$  the external field suppresses the gas-liquid transition in the Ising spin fluid, decreasing the critical temperature (lowering the top of binodal);<sup>12</sup> in the fluid with classical Heisenberg spins the field effect is nonmonotonic: weak fields lower the top of binodal, stronger fields shift the binodal up.<sup>22</sup> These various behaviors make it interesting to study the plane rotator model, which is in some respects intermediate between the Heisenberg and Ising models [see Eq. (1.5)], and also to compare the LG with the magnetic liquid, and thus investigate the effect of the underlying discretization.

In this paper we study the plane-rotator lattice gas using various theoretical approaches, i.e., mean-field (MFA) and two-site cluster (TCA) approximations, as well as Monte Carlo simulation. In Sec. II we calculate the thermodynamic potentials of the model within MFA and TCA, and the resulting phase diagrams, for selected values of the relevant parameters, are presented and discussed in Sec. III.

Since the resulting phase diagrams depend on a number of parameters, we decided to apply Monte Carlo simulation to a few specific values of them, so as to obtain a quantitative test of both the approximations, as well as a more detailed description. The simulation methodology is presented in Sec. IV, and in Sec. V its results are discussed and compared with MFA and TCA treatments. Conclusions are summarized in Sec. VI.

## II. MEAN-FIELD AND TWO-SITE CLUSTER TREATMENTS

Let us start from the explicit Hamiltonian of the plane rotator LG in an external (ordering) field, i.e.,

$$\begin{aligned} \Lambda = & - \frac{1}{2} \epsilon \sum_{j,k} \nu_j \nu_k \mathbf{u}_j \cdot \mathbf{u}_k - \mathbf{h} \cdot \sum_j \nu_j \mathbf{u}_j \\ & - \frac{1}{2} \lambda \sum_{j,k} \nu_j \nu_k - \mu \sum_j \nu_j; \end{aligned} \quad (2.1)$$

here  $j, k = 1 \cdots V$  enumerate sites of the simple cubic lattice,  $V$  is the total number of sites, and  $\mathbf{u}_k = (u_k^x, u_k^y)$  is a two-component unit vector.

The Hamiltonian [Eq. (2.1)] can be interpreted as describing a two-component system consisting of interconverting ‘‘real’’ ( $\nu_k = 1$ ) and ‘‘ghost,’’ ‘‘virtual’’ or ideal-gas particles ( $\nu_k = 0$ ); both kinds of particles have the same kinetic energy,  $\mu$  denotes the excess chemical potential of ‘‘real’’

particles over “ideal” ones, and the total number of particles equals the number of available lattice sites. The partition function is

$$Z = \text{Tr} \exp(-\beta\Lambda), \quad \beta = 1/(k_B T), \quad (2.2)$$

where the trace implies summation over all occupation patterns and integration over all spin orientations

$$\text{Tr} X = \sum_{\nu_1=0,1} \int \frac{d\phi_1}{2\pi} \cdots \sum_{\nu_V=0,1} \int \frac{d\phi_V}{2\pi} X. \quad (2.3)$$

Qualitative features of the model can be estimated using the MFA; probably, the simplest way to implement it involves decomposing the variables  $\nu_j$  and  $\mathbf{u}_k$  as follows:

$$\nu_j = \rho + \delta\rho_j, \quad \nu_j \mathbf{u}_j = \mathbf{M} + \delta\mathbf{M}_j, \quad (2.4)$$

$$\rho = \langle \nu_j \rangle_\Lambda, \quad \mathbf{M} = \langle \nu_j \mathbf{u}_j \rangle_\Lambda, \quad (2.5)$$

where  $\langle \cdots \rangle_\Lambda = [\text{Tr} \exp(-\beta\Lambda)]^{-1} \text{Tr} [\exp(-\beta\Lambda) \cdots]$  denotes a thermodynamic averaging. Upon substituting in Eq. (2.1), one obtains

$$\begin{aligned} \Lambda = & \frac{1}{2} V J_0 \mathbf{M} \cdot \mathbf{M} - \tilde{\mathbf{h}} \cdot \sum_i \nu_i \mathbf{u}_i + \frac{1}{2} V K_0 \rho^2 - \tilde{\mu} \sum_i \nu_i \\ & - \frac{1}{2} J_0 \sum_{ij} \delta\mathbf{M}_i \cdot \delta\mathbf{M}_j - \frac{1}{2} K_0 \sum_{ij} \delta\rho_i \delta\rho_j, \end{aligned} \quad (2.6)$$

where

$$J_0 = z\epsilon, \quad K_0 = z\lambda, \quad \tilde{\mathbf{h}} = \mathbf{h} + J_0 \mathbf{M}, \quad \tilde{\mu} = \mu + K_0 \rho. \quad (2.7)$$

Upon neglecting the terms quadratic in fluctuations appearing in Eq. (2.6), one obtains the effective Hamiltonian

$$\Lambda \rightarrow \Lambda^{\text{MFA}} = \frac{1}{2} V J_0 \mathbf{M} \cdot \mathbf{M} - \tilde{\mathbf{h}} \cdot \sum_i \nu_i \mathbf{u}_i + \frac{1}{2} V K_0 \rho^2 - \tilde{\mu} \sum_i \nu_i, \quad (2.8)$$

and hence the thermodynamic potential of the model within the MFA

$$\begin{aligned} \Omega = & -\beta^{-1} \ln \text{Tr} \exp(-\beta\Lambda^{\text{MFA}}) \\ = & -\beta^{-1} V \ln [1 + \exp(\beta\tilde{\mu}) i_0(\beta|\tilde{\mathbf{h}}|)] \\ & + \frac{1}{2} V J_0 \mathbf{M} \cdot \mathbf{M} + \frac{1}{2} V K_0 \rho^2; \end{aligned} \quad (2.9)$$

here  $i_m$  is a modified Bessel function of the first kind

$$i_m(x) = \frac{(-1)^m}{\pi} \int_0^\pi d\phi \exp(-x \cos \phi) \cos(m\phi). \quad (2.10)$$

By the underlying rotational invariance, the external field can be taken as defining a coordinate axis, say the  $x$  axis, i.e.,  $\mathbf{h} = (h, 0)$ , so that  $\mathbf{M} = (M, 0)$ ; minimization with respect to the two parameters  $\rho$  and  $M$  yields the self-consistency relations (2.5), i.e., a system of two nonlinear equations,

$$\rho = \frac{\exp(\beta\tilde{\mu}) i_0(\beta\tilde{h})}{1 + \exp(\beta\tilde{\mu}) i_0(\beta\tilde{h})}, \quad M = \frac{\exp(\beta\tilde{\mu}) i_1(\beta\tilde{h})}{1 + \exp(\beta\tilde{\mu}) i_0(\beta\tilde{h})}. \quad (2.11)$$

One can obtain thermodynamic quantities after solving the consistency equations (2.11) and calculating the thermodynamic potential (2.9).

The MFA fails to describe some phenomena connected with fluctuations. For example, it does not discern between the magnetic properties of systems with quenched and annealed disorder and does not describe percolation phenomena in quenched systems. This can partially be recovered using the idea of “clusters,” whereby the partition function of a finite group of particles in an external field can be evaluated explicitly. The contribution from “external” particles may be expressed in terms of the effective field, to be evaluated self-consistently. From such a point of view the MFA is a one-site cluster approximation, in which each cluster comprises one site. Increasing the size of clusters one may expect to obtain more accurate results. Indeed, the results of the two-site cluster approximation turn to be accurate for the one-dimensional systems<sup>29</sup> and on the Bethe lattice.<sup>30</sup> Below we shall formulate such an approximation for the lattice gas with the nearest-neighbor interactions. For the sake of brevity we shall not use the cluster expansion formulation which has some advantages, such as the possibility of calculating corrections of a higher order and correlation functions of the model.<sup>31</sup> Instead we shall rely on the first order approximation, which has been proven to give good quantitative agreement with Monte Carlo simulations for various lattice gas models (see, e.g., Ref. 32). Let us introduce the effective-field Hamiltonian of a single site

$$\Lambda_i = -\tilde{h} \nu_i u_i^x - \tilde{\mu} \nu_i, \quad (2.12)$$

where  $\tilde{h} = h + z\Phi$ ,  $\tilde{\mu} = \mu + z\Psi$ ,  $\Phi$  and  $\Psi$  are effective fields substituting for interactions with nearest-neighbor sites, and  $z$  is the first coordination number of the lattice. In the two-site Hamiltonian the interaction between a pair of the nearest-neighbor sites is taken into account explicitly

$$\begin{aligned} \Lambda_{ij} = & -\epsilon \nu_i \nu_j \mathbf{u}_i \cdot \mathbf{u}_j - \tilde{h}' \nu_i u_i^x - \tilde{h}' \nu_j u_j^x \\ & - \lambda \nu_i \nu_j - \tilde{\mu}' \nu_i - \tilde{\mu}' \nu_j, \end{aligned} \quad (2.13)$$

where  $\tilde{h}' = h + z'\Phi$ ,  $\tilde{\mu}' = \mu + z'\Psi$ , and  $z' = z - 1$ , since one of the neighbors is already taken into account. The variational parameters  $\Phi$  and  $\Psi$  have to be found from the self-consistency conditions that require an equality of average values calculated with the one-site and two-site Hamiltonians. To determine  $\Phi$  and  $\Psi$  it is sufficient to impose these conditions on the average values of spin  $M = \langle \nu_i u_i^x \rangle_\Lambda$  and of occupation number  $\rho = \langle \nu_i \rangle_\Lambda$ ,

$$\langle \nu_i \rangle_{\Lambda_i} = \langle \nu_i \rangle_{\Lambda_{ij}}; \quad \langle \nu_i u_i^x \rangle_{\Lambda_i} = \langle \nu_i u_i^x \rangle_{\Lambda_{ij}}. \quad (2.14)$$

The TCA leads to the following expression for the internal energy:

$$U/V = \langle \Lambda + \mu N \rangle / V = -\frac{1}{2} J_0 \langle v_i v_j \mathbf{u}_i \cdot \mathbf{u}_j \rangle_{\Lambda_{ij}} - h \langle v_i u_i^x \rangle_{\Lambda_{ij}} - \frac{1}{2} K_0 \langle v_i v_j \rangle_{\Lambda_{ij}}, \quad (2.15)$$

where  $J_0 = z\epsilon$  and  $K_0 = z\lambda$  are integral interaction strengths,  $J_0$  and  $K_0$  denote, respectively, the magnetic coupling and the nonmagnetic attraction between nearest-neighbor sites. Expression (2.15) can be computed explicitly in terms of the fields  $\Phi$  and  $\Psi$  and model parameters. The thermodynamic potentials can be found in a straightforward way. For example, the grand thermodynamic potential  $\Omega$  of the model satisfies the following Gibbs-Helmholtz equation:

$$\frac{\partial \beta \Omega}{\partial \beta} = U - \mu N. \quad (2.16)$$

Taking into account relations (2.14), the solution of this differential equation reads

$$\beta \Omega / V = z' \ln \text{Tr} \exp(-\beta \Lambda_i) - \frac{z}{2} \ln \text{Tr} \exp(-\beta \Lambda_{ij}). \quad (2.17)$$

The traces in expressions involving one-site and two-site Hamiltonians ( $\Lambda_i$  and  $\Lambda_{ij}$ ) are easily computable. Expressions (2.17) and (2.14) yield the thermodynamic potential

$$\beta \Omega / V = z' \ln Z_1 - \frac{z}{2} \ln Z_2, \quad (2.18)$$

and the self-consistency equations

$$\frac{x i_0(\beta \tilde{h})}{Z_1} = \frac{y i_0(\beta \tilde{h}') + y^2 \exp(\beta \lambda) L}{Z_2}; \quad (2.19)$$

$$\frac{x i_1(\beta \tilde{h})}{Z_1} = \frac{y i_1(\beta \tilde{h}') + y^2 \exp(\beta \lambda) L'}{Z_2}; \quad (2.20)$$

where  $x = \exp(\beta \tilde{\mu})$ ,  $y = \exp(\beta \tilde{\mu}')$ ,

$$Z_1 = 1 + x i_0(\beta \tilde{h}), \quad Z_2 = 1 + 2y i_0(\beta \tilde{h}') + y^2 \exp(\beta \lambda) L, \quad (2.21)$$

$$L = \int_0^{2\pi} \frac{d\phi_1}{2\pi} \int_0^{2\pi} \frac{d\phi_2}{2\pi} \exp[\beta \tilde{h}' (\cos \phi_1 + \cos \phi_2) + \beta \epsilon \cos(\phi_1 - \phi_2)] \\ = \int_0^{\pi} \frac{d\phi_1}{\pi} \exp[\beta \tilde{h}' \cos \phi_1] i_0 \left( \beta \sqrt{(\tilde{h}')^2 + \epsilon^2 + 2\tilde{h}' \epsilon \cos \phi_1} \right), \quad (2.22)$$

$$L' = \int_0^{2\pi} \frac{d\phi_1}{2\pi} \int_0^{2\pi} \frac{d\phi_2}{2\pi} \cos \phi_1 \exp[\beta \tilde{h}' (\cos \phi_1 + \cos \phi_2) + \beta \epsilon \cos(\phi_1 - \phi_2)] \\ = \int_0^{\pi} \frac{d\phi_1}{\pi} \cos \phi_1 \exp[\beta \tilde{h}' \cos \phi_1] i_0 \left( \beta \sqrt{(\tilde{h}')^2 + \epsilon^2 + 2\tilde{h}' \epsilon \cos \phi_1} \right). \quad (2.23)$$

The resulting phase diagrams are presented and discussed in the following sections. The reliability of MFA and TCA for the plane rotator lattice gas is also tested by computer simulations; this will be carried out for  $\lambda=0$  and for one value of the chemical potential,  $\mu=0.1$ , yielding a rather detailed description of static properties.

### III. MEAN-FIELD AND TWO-SITE CLUSTER PHASE DIAGRAMS

Figure 1 shows phase diagrams of the plane rotator lattice gas within the TCA and the MFA. First note the two regions in the temperature-density space: at high temperatures and low densities the system is paramagnetic (P region), whereas at low temperatures and high densities the spontaneous orientational order appears ( $\mathbf{M} \neq 0$ ) and the system is ferromagnetic (F region). The boundary between these regions (the Curie line) is a locus of Curie points, where the second order phase transitions take place. At positive  $\mu$  (e.g.,  $\mu=0.1$ , see the thin line in Fig. 1) the dependence  $\rho(t)$  (where  $t = k_B T / J_0$ ) is smooth except a jump of slope at the intersec-

tion with the Curie line. For sufficiently small  $\mu$  (see  $\mu = -1.2$  in Fig. 1) the dependence  $\rho(t)$  contains a jump showing discontinuous (first order) transition between ferromagnetic and paramagnetic phases. The bold convex line resting on the points (0,0) and (1,0) in the phase diagram is a binodal, which confines the region B, where the homogeneous lattice gas is unstable (or metastable) and must separate into phases of different densities. As a result,  $\rho(t)$  lines jump over this region. Within the magnetofluid interpretation of the current model the binodal separates the liquid and vapor (gaseous) phases. One can see that at  $\lambda=0$  the vapor is always paramagnetic and the liquid is always ferromagnetic. Above the top of the binodal [ $t > 0.25$  (MFA) or  $t > 0.201$  (TCA)] there is no gas-liquid transition, but the orientational transition survives up to  $t=0.5$  (MFA) (or  $t=0.406$  within TCA). Comparing the TCA phase diagram (thick solid lines in Fig. 1) with the MFA result (dashed lines) one can see that fluctuations taken into account within the TCA significantly lower both the binodal and the Curie line.

Figure 2(a) shows the temperature-density phase diagram of the model within the MFA at different model parameters.

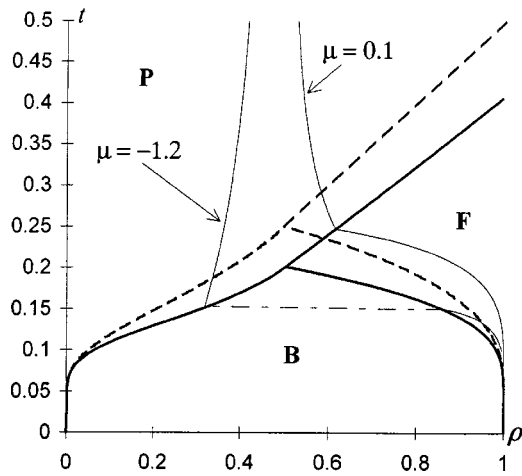


FIG. 1. The dependence of density ( $\rho=N/V$ ) on temperature ( $t=k_B T/J_0$ ) at constant chemical potential  $\mu$  (thin lines) and phase diagram (thick solid lines) of plane-rotator lattice gas at  $\lambda=0$  within the TCA. Thin long-short-dashed line represents the jump of density at  $\mu=-1.2, t=0.15$ . Symbols P, F, and B mark paramagnetic, ferromagnetic, and binodal regions, respectively. Dashed lines represent the phase diagram within the MFA.

One can see how the nonmagnetic attraction and external field change the phase diagram. There are three families of lines for three values of the nonmagnetic interaction strength  $v=\lambda/\epsilon=K_0/J_0$ . The bold lines correspond to the zero-field case ( $h=0$ ). One can see that the Curie lines corresponding to different  $v$  overlap, because within the MFA the Curie points lay on the straight line and its slope is independent of  $v$ . The nonmagnetic attraction between particles, of course, favors the phase separation—the binodal moves upward with increasing  $v$ . At small  $v$  the top of binodal lays on the Curie

line, the liquid is ferromagnetic and the gas is paramagnetic. At large  $v$  the top of binodal deviates from the Curie line in the paramagnetic region.

The external field destroys the ferromagnetic transition and therefore eliminates the Curie line. The gas-liquid binodals in presence of the external magnetic field are depicted with thin lines. The attached numbers are strengths of the field  $h/J_0$ . At  $v=0$  the field effect is nonmonotonic—as the strength of field grows, first the top of binodal lowers ( $h=0.01J_0, 0.1J_0$ ), but then it begins to raise ( $h=0.5J_0, \infty$ ). Thus, the gas-liquid critical temperature (which is the ordinate of the binodal top) is a nonmonotonic function of the field. At  $v=1$  this phenomenon remains, but the effect of the binodal lowering weakens. At large  $v$  (e.g.,  $v=2$ ) the binodal lowering disappears and the external field monotonically raises the binodal.

In Fig. 2(b) one can see that the TCA yields quantitative differences, as well as some qualitative corrections to the MFA results. Within the TCA the Curie line becomes slightly concave, and the nonmagnetic attraction between particles increases the Curie temperature. The latter effect can be justified by qualitative arguments. Indeed, the nonmagnetic attraction augments the probability that a randomly chosen pair of nearest-neighbor sites is occupied. Since at these sites the particles interact magnetically, the magnetic interaction becomes more efficient, and the Curie temperature increases too. The MFA does not capture this effect because it completely disregards the last two terms in Eq. (2.6) which describe the interaction of fluctuations. Taking into account of density fluctuations in the TCA leads to the dependence of the Curie temperature on  $v$ . When  $\mu \rightarrow +\infty$  the lattice is saturated, ( $\rho \rightarrow 1$ ), density fluctuations are absent, and the Curie temperature becomes independent of the nonmagnetic attraction.

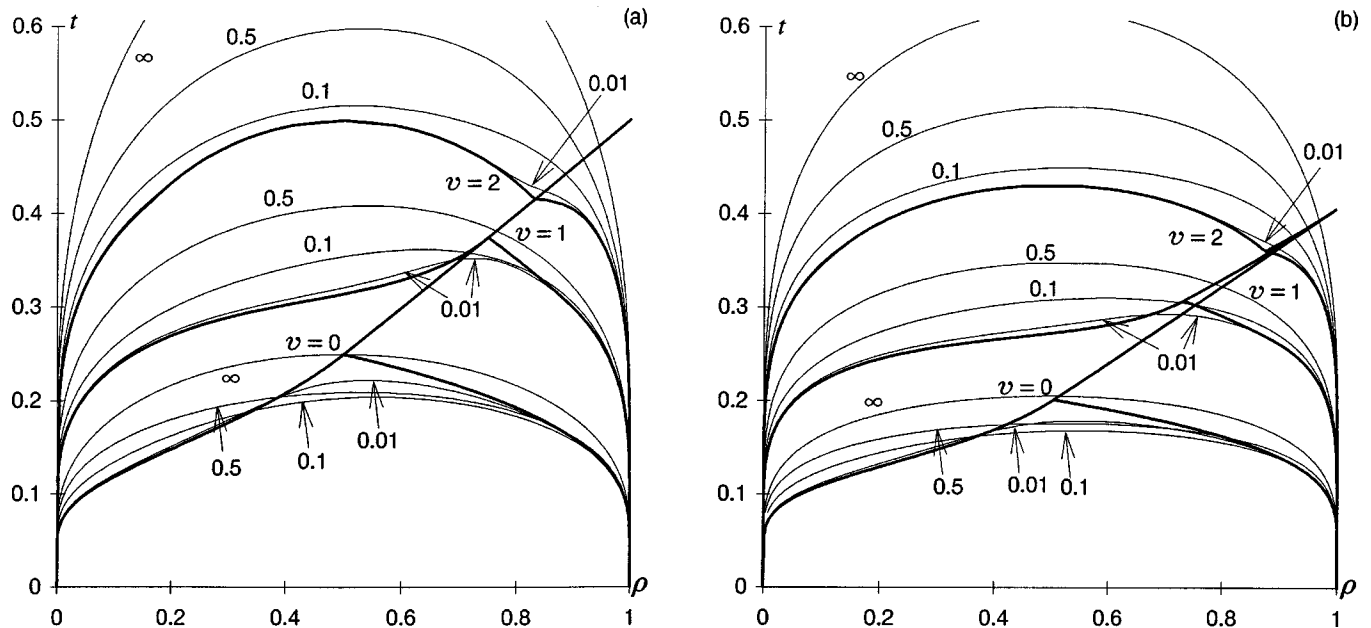


FIG. 2. Phase diagrams of the plane-rotator lattice gas within the mean-field (a) and two-site cluster (b) approximations. Picture (b) represents TCA results for the model with the nearest-neighbor interactions on the simple cubic lattice ( $z=6$ ). The MFA results [picture (a)] are independent of interaction range and lattice structure. Three families of lines are built for three values of nonmagnetic interaction  $v=K_0/J_0$ . The thick lines are binodals and Curie lines at zero external field. The thin lines with attached numbers represent the binodals at nonzero values of the external field  $h/J_0$ .

TCA predictions concerning the effect of the field support the MFA results. Taking into account that the MFA is accurate in the limit of Kac potentials<sup>33</sup> one can be sure that the observed  $v$  dependence of phase diagrams and field effects does take place for systems with long-range potentials. The TCA captures main features of systems with nearest-neighbor interactions and makes us think that these effects survive also in models with short-range interactions.

The observed variety of field effects may be explained by the existence of two concurrent tendencies.<sup>12,22</sup> On the one hand, the external field aligns the spins, leading to a more efficient attraction between particles [let us recall that magnetic interaction between particles with nearly parallel spins ( $\mathbf{u}_i \cdot \mathbf{u}_j > 0$ ) leads to their attraction, whereas particles with opposite spins ( $\mathbf{u}_i \cdot \mathbf{u}_j < 0$ ) repel each other]. This raises the binodal (for example, in simple nonmagnetic fluids the binodal goes up when the interaction increases). On the other hand, if the susceptibility of the rarefied phase is larger than that of the coexisting dense phase, then magnetization and, consequently, effective attraction between particles grow better in the rarefied phase, thus decreasing the energetical gain of the phase separation. Therefore the second tendency suppresses the gas-liquid separation in the fluid and counteracts the first tendency. The second tendency is very strong at  $h=0$  and  $v=0$  near the top of binodal, because in this case the vapor (paramagnetic) branch of binodal almost coincides with the Curie line (where the susceptibility tends to infinity), whereas the branch of the coexistent liquid phase rapidly deviates from the Curie line. As a result, the external field lowers the top of the binodal. If both the liquid and vapor phases are paramagnetic, the susceptibility of the liquid phase is larger, and the second (lowering) tendency is absent. The behavior of the binodal for  $v=2$  (see Fig. 2) demonstrates this feature. Other factors can also change a relation between the susceptibilities. For example, a short-range character of the interactions levels the susceptibilities and weakens the lowering tendency,<sup>22</sup> as can be observed from the field effect at  $v=1$ : in Fig. 2(a) (the MFA result) the top of binodal at  $h=0$  is higher than that at  $h=0.1J_0$ , whereas in Fig. 2(b) (TCA) these binodals have nearly equal heights. Since the MFA results are correct for long-range potentials, whereas for the model with nearest-neighbor interactions the TCA is much more accurate, the corrections provided by the TCA have to be attributed to differences between the systems with the long-range and short-range potentials.

Comparing different spin fluids one can note that the role of the binodal lowering tendency decreases in the sequence: Ising, plane rotator, Heisenberg fluids. This follows from the observation of the effect of the field in fluids without the nonmagnetic attraction ( $v=0$ ): in the Ising LG<sup>12</sup> the external field monotonically decreases the critical temperature  $t_c$  (lowers the top of the gas-liquid binodal); in the plane rotator LG (see Fig. 2) weak fields lower  $t_c$ , but at larger fields the increasing tendency wins, so that  $t_c(h=\infty)$  is nearly equal to  $t_c(h=0)$ , and  $t_c$  is minimal at a finite value of the field; in the Heisenberg fluid<sup>22</sup> the increasing tendency is still more pronounced:  $t_c(h=\infty)$  is much higher than  $t_c(h=0)$ .

At intermediate  $v$  (e.g.,  $v=1.5$ ) phase diagrams of a special topology appear, similar to those previously reported for the Ising lattice gas,<sup>18</sup> as well as off-lattice Ising-van der

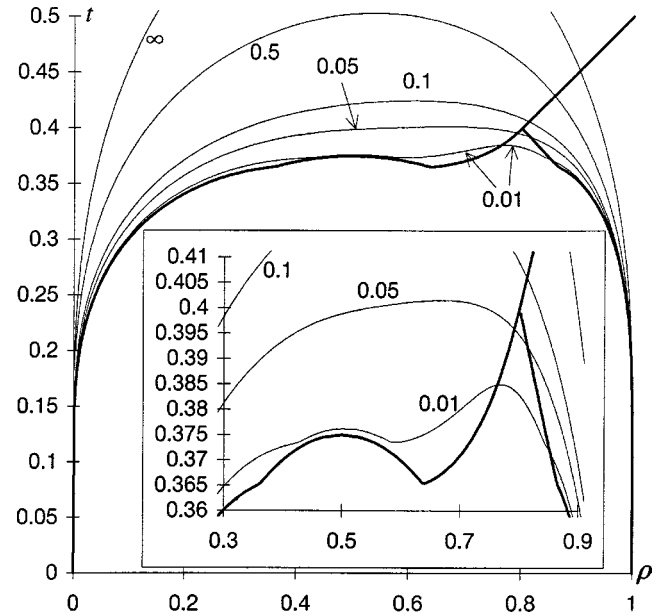


FIG. 3. Phase diagram of the model at  $v=1.5$  within the MFA. Thick lines correspond to  $h=0$ ; thin lines are binodals at different values of external field  $h/J_0$  (see attached numbers). The inset shows details of the upper part of  $h=0$  binodal.

Waals<sup>21,28</sup> and dipolar<sup>23,24</sup> fluids. Within the MFA [Fig. 3(a)] our model at  $h=0$  and  $t=0.37$  undergoes two first-order phase transitions. At this temperature the fluid can be in three phases: paramagnetic gas (at  $\rho < 0.40$ ), paramagnetic liquid ( $0.6 < \rho < 0.69$ ) and ferromagnetic liquid ( $\rho > 0.86$ ). The TCA predicts the similar phase diagram (not reported here). We would like to emphasize that weak external fields (e.g.,  $h/J_0=0.01$ ) raise the binodal at  $\rho=0.5$  and lower it at  $\rho=0.8$ . Such a behavior completely fits into the ‘‘bitendency’’ explanation: at  $\rho=0.5$  and  $h=0$  both phases are paramagnetic, the lowering tendency is absent, therefore the external field favors the phase separation; at  $\rho=0.8$  the lowering tendency wins at small fields, like in the case  $v=1$  (see Fig. 2).

#### IV. SIMULATION

LG models involving continuous spins [Eq. (1.4)] have seldom been studied by simulation,<sup>34</sup> in contrast with their SL counterparts, and with LG models with discrete spins.

The simulation step used here consisted of different consecutive stages, as discussed in detail in Ref. 34; each of them being attempted irrespectively of the outcome of the previous ones; the methodologies used here have been discussed and then applied in a number of papers, both for lattice and off-lattice models, (e.g., Refs. 35–46), as well as reviewed in standard reference books on simulation,<sup>47–49</sup> some recent grand-canonical or semi-grand-canonical simulations can be found in Refs. 50 and 51.

The stages are (a) canonical attempt on a randomly chosen site, supplemented by overrelaxation;<sup>52–55</sup> and (b) semi-grand-canonical<sup>51</sup> attempt: a lattice site  $k$  is chosen randomly, and an attempt is made to change  $\nu_k$  to  $\nu'_k$ , i.e., from zero to one or vice versa; the quantity involved in the Metropolis procedure is now

$$\Delta\Lambda = -\Delta N(\mathbf{B}_k \cdot \mathbf{u}_k + \mu), \quad \Delta N = \nu'_k - \nu_k, \quad (4.1)$$

where  $\mathbf{B}_k = \sum_j' \nu_j \mathbf{u}_j$  denotes the local field produced by the nearest neighbors. Note that particles are distinguishable, and that the choice of a strict grand-canonical interpretation would require adding a kinetic-energy term  $Nk_B T/2$  in Eq. (1.4), and hence the corresponding term  $\Delta Nk_B T/2$  in Eq. (4.1).

In addition to these basic stages, it was sometimes found beneficial to implement two more: (c) another canonical attempt; and (d) exchange of places between ‘‘real’’ and ‘‘virtual’’ particles: a pair of lattice sites  $j$  and  $k$ , such that  $\nu_j \neq \nu_k$ , is chosen randomly, and an attempt is made to swap the two ‘‘particles.’’<sup>36,37,56</sup>

Simulations were carried out on periodically repeated cubic samples, consisting of  $V = L^3$  sites,  $L = 12, 16, 20$ . Equilibration runs took between 25 000 and 50 000 cycles (where one cycle or sweep involves  $V$  steps), and production runs for estimating ensemble averages took between 100 000 and 250 000; macrostep averages for evaluating statistical errors were taken over 1000 cycles.

Calculations were carried out in cascade, in order of increasing temperature; as an additional check, a few runs were carried out in order of decreasing temperature, and both the procedures found to yield the same results to within statistical errors.

Calculated observables include mean Hamiltonian (or total energy) per site and its temperature derivative (specific heat at constant  $\mu$  and  $V$ ), density and its derivative with respect to the chemical potential, defined by

$$\bar{H} = (1/V) \langle \Lambda \rangle, \quad (4.2)$$

$$\rho = (1/V) \langle N \rangle, \quad (4.3)$$

and by the fluctuation formulas<sup>35,43,57,58</sup>

$$\rho_\mu = (\partial \rho / \partial \mu)_{TV} = (\beta/V) [\langle N^2 \rangle - \langle N \rangle^2], \quad (4.4)$$

$$\frac{C_{\mu V}}{k_B} = \frac{1}{k_B V} \left( \frac{\partial \langle \Lambda \rangle}{\partial T} \right)_{\mu V} = (\beta^2/V) [\langle \Lambda^2 \rangle - \langle \Lambda \rangle^2]. \quad (4.5)$$

We also calculated mean magnetic moment per site, magnetic susceptibility, as well as first- and second-rank orientational order parameters (per spin), and singlet orientational distribution function. The magnetization (per site) is defined by

$$M = (1/V) \langle \sqrt{\mathbf{F} \cdot \mathbf{F}} \rangle, \quad \mathbf{F} = \sum_k \nu_k \mathbf{u}_k; \quad (4.6)$$

as for the susceptibility  $\chi$ , let us first define the two quantities

$$\chi_1 = \frac{\beta}{V} (\langle \mathbf{F} \cdot \mathbf{F} \rangle - \langle |\mathbf{F}| \rangle^2), \quad (4.7)$$

$$\chi_2 = \frac{\beta}{V} \langle \mathbf{F} \cdot \mathbf{F} \rangle; \quad (4.8)$$

the susceptibility per site is defined by

$$\chi = \beta \lim_{V \rightarrow \infty} \frac{1}{V} (\langle \mathbf{F} \cdot \mathbf{F} \rangle - \langle \mathbf{F} \rangle \cdot \langle \mathbf{F} \rangle), \quad (4.9)$$

but it has been shown (see, e.g., Refs. 59 and 60) that, in simulation, its finite-lattice estimates are given by

$$\chi = \begin{cases} \chi_1, & \text{in the ordered region,} \\ \chi_2, & \text{in the disordered region.} \end{cases} \quad (4.10)$$

Let us also note that, for an arbitrary configuration, the quantity  $\mathbf{F}$  defines a unit vector  $\mathbf{f} = \mathbf{F}/|\mathbf{F}|$ ; one can then define

$$s_1 = \frac{1}{N} \sum_k \nu_k (\mathbf{u}_k \cdot \mathbf{f}), \quad s_2 = \frac{1}{N} \sum_k \nu_k [2(\mathbf{f} \cdot \mathbf{u}_k)^2 - 1] \quad (4.11)$$

and hence  $\bar{s}_1$  and  $\bar{s}_2$ ; notice that  $\bar{s}_1$  differs from  $M$  by the density  $\rho$ . Moreover, one can construct the singlet orientational distribution function<sup>61–63</sup> (SODF)  $S(\phi)$  for individual spins around the magnetization vector  $\mathbf{f}$ , where  $\phi$  is the angle between the individual spin and the magnetization unit vector  $\mathbf{f}$ , ranging between 0 and  $\pi$ . This was evaluated at  $t = 0.23$ , on a sample of  $V = 20^3$  sites, by analyzing a configuration every fourth cycle and producing a 1001 bin histogram. Note also that the SODF is usually considered for the nematocounterparts.<sup>61–63</sup>

A cubic sample of  $V$  sites contains  $zV/2 = 3V$  distinct nearest-neighbor pairs of lattice sites; we worked out pair occupation probabilities, i.e., the mean fractions  $P_{\xi\eta}$  of pairs being both empty ( $P_{ee} = \langle (1 - \nu_i)(1 - \nu_k) \rangle$ ), both occupied ( $P_{oo} = \langle \nu_i \nu_k \rangle$ ), or consisting of an empty and an occupied site ( $P_{eo} = 1 - P_{oo} - P_{ee}$ ). Orientational order at short range was defined by means of the quantities

$$C_m = \langle (\nu_j \nu_k) \cos[m(\phi_j - \phi_k)] \rangle_{nn}, \quad m = 1, 2 \quad (4.12)$$

at nearest-neighbor separation; the mean interaction energy per site is just  $-(z/2)(\epsilon C_1 + \lambda P_{oo})$ .

In order to allow for the possibility of staggered positional order, we evaluated

$$\sigma = (2/V) \left\langle \sum_k \nu_k q_k \right\rangle, \quad (4.13)$$

and found it to be essentially zero, in keeping with the absence of purely positional terms in the interaction potential.

The positional correlation function

$$h(r) = \langle \nu_j \nu_k \rangle, \quad (4.14)$$

as a function of the distance between sites  $j$  and  $k$ ,  $r = |\mathbf{x}_j - \mathbf{x}_k|$ , was calculated for  $L = 20$  and at a few temperatures, i.e.,  $t = 0.23$  and  $t = 0.25$ , together with its orientational counterparts

$$\Gamma_m(r) = G_m(r)/h(r),$$

$$G_m(r) = \langle (\nu_j \nu_k) \cos[m(\phi_j - \phi_k)] \rangle, \quad m = 1, 2. \quad (4.15)$$

## V. SIMULATION RESULTS

It is generally known that mean field theories underestimate fluctuations. This, as a rule, leads to overestimation of a range of existence of ordered phases, in particular, to overestimation of the order-disorder transition temperature. Sometimes, this leads to qualitatively incorrect results. For example, the MFA does not describe percolation phenomena

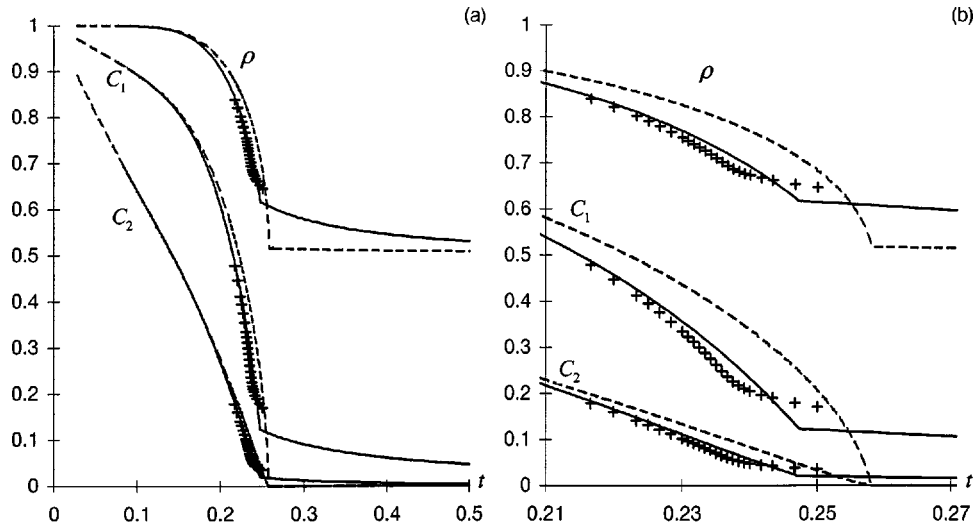


FIG. 4. Temperature dependence of the density  $\rho$  and orientational short-range order parameters  $C_1$ ,  $C_2$ . Simulation estimates obtained with different sample sizes were found to agree to within the statistical errors, so that we just plot here their averages over the examined sample sizes (crosses). Solid and dashed lines represent the results of the TCA and the MFA, respectively. Results in all the figures of this section refer to  $\lambda=0$ , and  $\mu=0.1$ .

in *quenched* LG with magnetic nearest-neighbor interactions (i.e., whose translational degrees of freedom are frozen, since both number and positions of particles are fixed), where it wrongly predicts the existence of spontaneous magnetic order at *any* density. In any *annealed* spin LG both orientation and density fluctuations are present. We want to know whether they and their correlations cause significant difficulties for the mean field theories. Fluctuations are especially large near second-order phase transitions, and therefore we test both the MFA and the TCA in the ferromagnetic (second-order) transition region.

In this section we present theoretical and simulation results for the plane rotator model defined by  $\lambda=0$  and  $\mu=0.1$ . MC results for a number of observables, such as  $\bar{H}$  (not reported here),  $\rho$ ,  $C_m$ ,  $P_{\xi\eta}$  were found to evolve with temperature in a smooth way, and to be independent of sample sizes; in these cases, we simply plotted the averages over the examined sample sizes; other quantities ( $C_{\mu\nu}$ ,  $\rho_\mu$ , and the susceptibility, not shown here) demonstrate a more pronounced sample-size dependence, especially around the transition temperature  $t \approx 0.237$ . The named approximate treatments predict ferromagnetic order-disorder transition at  $t_C=0.247$  (TCA) or  $t_C=0.258$  (MFA). Results for density  $\rho$  and orientational short-range order parameters  $C_1$  and  $C_2$  are reported in Fig. 4. In Fig. 4(a) one can see that there is a good agreement between the theories and the MC simulations in the ferromagnetic phase. Discrepancies appear only near the Curie temperature  $t_C$ . In Fig. 4(b) this critical region is shown in detail, and one can see that the TCA results are much more accurate than those of the MFA. For example, within the TCA the Curie temperature, [corresponding to a jump in the slope of the  $\rho(t)$  plot in Fig. 4] agrees with the simulation prediction to about 4% (vs 9% for the MFA). The density at which orientational transition takes place  $\rho_C=0.616$  is also much closer to the MC value  $\rho_C \approx 0.68$  than the MFA result  $\rho_C=0.520$ . Note that, according to both simulations and TCA, the orientational short-range order parameters  $C_1$ ,  $C_2$  do not vanish in the paramagnetic phase, in

contrast to the MFA where they equal zero. In Fig. 5 the pair occupation probabilities  $P_{\xi\eta}$  are presented. One can see that there is a satisfactory quantitative agreement between simulation estimates and TCA results. The MFA results are rather in qualitative agreement with the simulations. Drawbacks of the MFA become more visible in Fig. 6 where we present correlation functions. Positional nearest-neighbor correlations of particles are described by the quantity  $h(1)-h(\infty)=P_{oo}-\rho^2$  [Fig. 6(a)]. Let us note that the corresponding particle-hole and hole-hole correlations [described by  $P_{eo}/2-\rho(1-\rho)$  and  $P_{ee}-(1-\rho)^2$ ] are not independent quantities because

$$P_{oo}-\rho^2=-[P_{eo}/2-\rho(1-\rho)]=P_{ee}-(1-\rho)^2. \quad (5.1)$$

Quantities that describe the nearest-neighbor orientational correlations  $\Gamma_m(1)-\Gamma_m(\infty)$  are presented in Fig. 6(b). One can see that the MFA prediction for these quantities is zero. The quantity  $\Gamma_1(1)-\Gamma_1(\infty)=C_1/P_{oo}-s_1^2$  has a peak at the

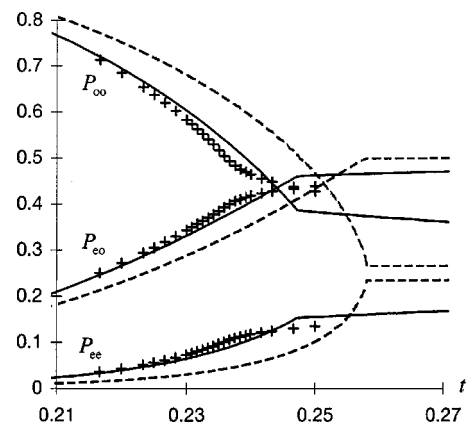


FIG. 5. Simulation estimates (crosses), results of the TCA (solid lines) and the MFA (dashed lines) for pair occupation probabilities  $P_{oo}$ ,  $P_{eo}$ ,  $P_{ee}$ ; see also Fig. 4, and see the text for their definitions.

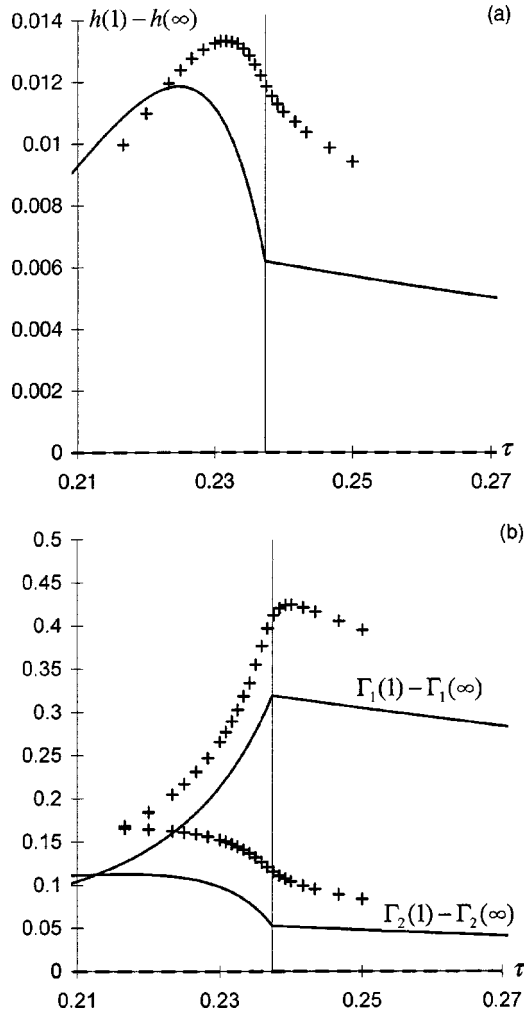


FIG. 6. Simulation estimates (crosses) and results of TCA (solid lines) and MFA (dashed lines) for the nearest-neighbor correlation functions  $h(1) - h(\infty)$  (a) and  $\Gamma_m(1) - \Gamma_m(\infty)$  (b) plotted against the scaled temperature  $\tau$  ( $\tau = t$  for MC results,  $\tau = 0.96t$  for the TCA, and  $\tau = 0.92t$  for the MFA). The thin vertical line marks the Curie temperature.

Curie point, where the system loses orientational stability and simulation estimates for the magnetic susceptibility show a pronounced increase with increasing sample size, pointing to its divergence in the thermodynamic limit. On the other hand, the quantity  $\Gamma_2(1) - \Gamma_2(\infty) = C_2/P_{oo} - \bar{s}_2^2$  does not have a maximum at phase transition since  $\bar{s}_2$  is far less affected by the ordering transition.

Strong orientational correlations near the Curie temperature enhance density correlations, as manifested by the peak of the nearest-neighbor correlation function  $h(1) - h(\infty)$  [Fig. 6(a)]. Note that at  $\mu = 0.1$  the system remains mechanically stable at all temperatures (since the compressibility  $\mathcal{L} = \rho_\mu/\rho$  is always finite, as can be seen in Fig. 9) and we have only the orientational phase transition of the second order.

We have also shown in a previous section that large density fluctuations near the Curie point result in the gas-liquid transition at a smaller  $\mu$ . Let us note that both the simulations and the TCA predict that the peak of nearest-neighbor positional correlation function [Fig. 6(a)] is somewhat

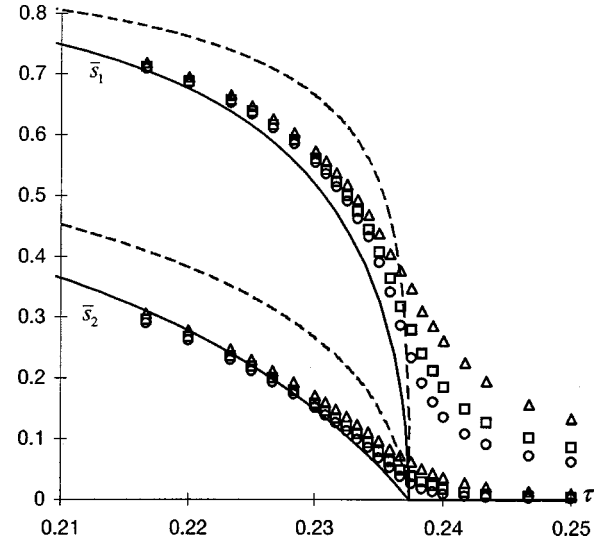


FIG. 7. Simulation estimates for the first-rank and second-rank order parameters obtained with different sample sizes: triangles:  $L = 12$ ; squares:  $L = 16$ ; circles:  $L = 20$ . Solid and dashed lines are the results of the TCA and the MFA, respectively.

shifted to lower temperatures and lays in the ferromagnetic phase.

Figure 7 presents the temperature dependence of long-range orientational order parameters. In order to compare curve shapes within different approximations we plot these quantities against the scaled temperature  $\tau$  ( $\tau = t$  for MC results,  $\tau = 0.96t$  for the TCA and  $\tau = 0.92t$  for the MFA). Similarly we plot the specific heat  $C_{\mu V}$  (Fig. 8), and  $\rho_\mu$  (Fig. 9). All the figures again show good quantitative agreement between the MC and the TCA and qualitative agreement with the MFA.

A less severe comparison between MFA prediction and simulation results can be obtained by plotting  $\bar{s}_2$  versus  $\bar{s}_1$ , thus eliminating their explicit temperature dependences; this is done in Fig. 10, which again shows a reasonable agree-

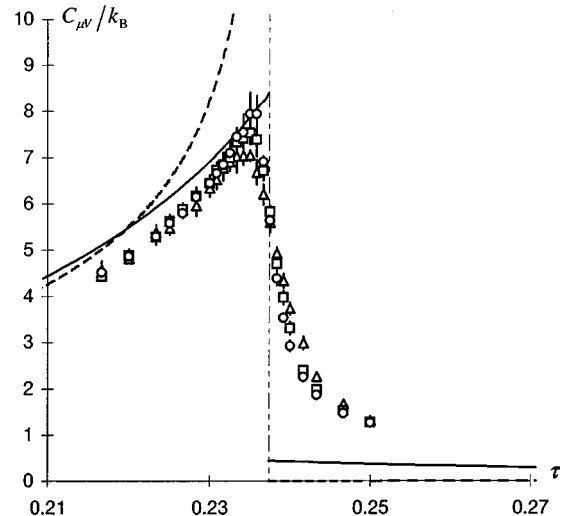


FIG. 8. Simulation estimates, obtained with different sample sizes, and theoretical results for the specific heat per site; same notations as in Fig. 7. Thin long-short-dashed line represents the jump of  $C_{\mu,V}/k_B$  at the Curie temperature.

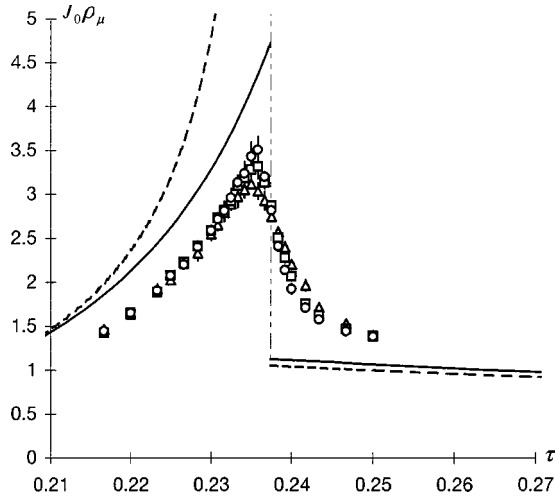


FIG. 9. Simulation estimates, obtained with different system sizes, and theoretical results for  $J_0\rho_\mu$ ; same notations as in Fig. 7. Thin long-short-dashed line represents the jump of  $J_0\rho_\mu$  at the Curie temperature.

ment; notice that MFA predicts for the SODF the maximum-entropy expression  $S_{MF}(\phi) = S_{ME,1}(\phi) \propto \exp(A_1 \cos \phi)$ , (see below), so that the MFA plot was obtained by calculating  $\bar{s}_1$  and  $\bar{s}_2$  over a wide range of  $A_1$ .

The SODF (calculated at  $t=0.23$ , and not shown here)<sup>61–63</sup> can be formally expanded as

$$S(\phi) \propto \exp\left[\sum_{m>0} A_m \cos(m\phi)\right] \\ = (1/\pi) \left[1 + 2 \sum_{k>0} \bar{s}_k \cos(k\phi)\right], \quad (5.2)$$

where  $\phi$  is the angle between the individual spin and the magnetization vector, ranging between 0 and  $\pi$ , and the coefficients  $\bar{s}_k$  define order parameters.

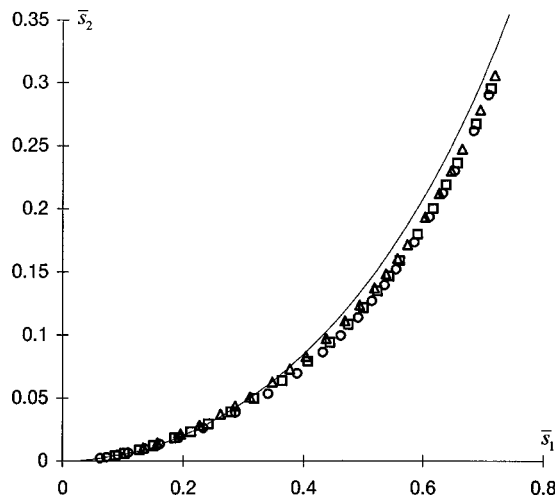


FIG. 10. Plots of second-rank order parameter versus first-rank order parameter, obtained with different sample sizes; same meaning of symbols as in Fig. 7; the thin line is the mean-field prediction, i.e., corresponding to a singlet distribution  $S_{MF}(\phi) = S_{ME,1}(\phi) \propto \exp(A_1 \cos \phi)$ .

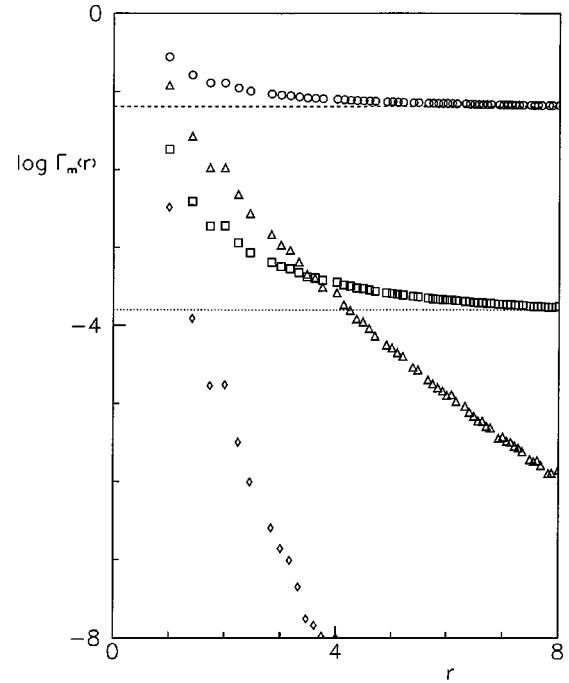


FIG. 11. Simulation estimates for  $\Gamma_m(r)$  obtained with  $L=20$  and at different temperatures: circles:  $\Gamma_1(r)$  at  $t=0.23$ ; squares:  $\Gamma_2(r)$  at  $t=0.23$ ; triangles:  $\Gamma_1(r)$  at  $t=0.25$ ; diamonds:  $\Gamma_2(r)$  at  $t=0.25$ ; the dashed line corresponds to the square of  $\bar{s}_1$ , and the dotted one to the square of  $\bar{s}_2$ .

Both the simulated  $S(\phi)$  and its maximum entropy estimates,<sup>64–66</sup> based on  $\bar{s}_1$  and  $\bar{s}_2$ , were found to decrease monotonically with increasing  $\phi$ ; the maximum entropy estimates are defined by

$$S_{ME,1}(\phi) \propto \exp(A_1 \cos \phi), \quad (5.3)$$

$$S_{ME,2}(\phi) \propto \exp[B_1 \cos \phi + B_2 \cos(2\phi)]; \quad (5.4)$$

here proportionality factors allow for normalization conditions, and  $A$  or  $B$  parameters were determined by appropriate consistency constraints, i.e., by requesting  $S_{ME,1}$  to reproduce  $\bar{s}_1$ , or requesting  $S_{ME,2}$  to reproduce both  $\bar{s}_1$  and  $\bar{s}_2$ ,<sup>64–66</sup> notice also that MFA predicts the functional form  $S_{MF}(\phi) = S_{ME,1}(\phi)$ .

For  $S_{ME,2}(\phi)$ , we found  $B_1 = 1.392$ ,  $B_2 = -0.067$ , i.e.,  $B_2$  turned out to be small but not negligible: comparisons showed that  $S_{ME,1}$  yields a good but not perfect agreement with simulation results, and that  $S_{ME,2}$  produces a recognizable improvement.

As for correlation functions,  $h(r)$  (not reported) was found to quickly decay to its long-range limit  $\rho^2$ , reflecting the fact that  $\lambda=0$ , i.e., the absence of purely positional interactions. Simulation results for the orientational correlation functions are plotted in Fig. 11; note that both  $h(r)$  and  $\Gamma(r)$  have a maximum at  $r=2$ , similar to that in off-lattice fluids. In LGs the effect probably correlates with the fact that the path along the lattice bonds to the fourth coordination shell ( $r=2$ ) is shorter (two steps) than that to the third one (three steps,  $r=\sqrt{3}$ ). The same peak is observed in off-lattice fluids

(near separation of two hard core diameters), and just suggests hidden geometrical effects resulting from short-range order in real fluids.

## VI. CONCLUSIONS

We have performed a study of the plane-rotator lattice gas, based on theoretical methods: MFA and TCA have been used to construct overall phase diagrams, and to investigate field effects; computer simulation has been used for  $\lambda=0$  and  $\mu=0.1$ , as a mean to assess the quantitative accuracy of both MFA and TCA, and also to obtain a more detailed description. The theories appear to be able to describe thermodynamic properties of the model with nearest-neighbor interactions with satisfactory accuracy: the MFA is in qualitative agreement with the simulation results, the TCA gives a good quantitative description. For example, in the case considered in Sec. V the temperature of orientational ordering predicted by the TCA (MFA) agrees with the simulation result to about 4% (9%). The TCA also manages to describe nearest-neighbor correlations, which makes this theory useful for description of scattering data. Near the Curie temperature, simulation as well as TCA results show the significant growth of nearest-neighbor correlations for both orientational and density fluctuations [ $\Gamma_1(1)-\Gamma_1(\infty)$  and  $h(1)-h(\infty)$ , respectively], and also the onset of long-range orientational correlations ( $\chi \rightarrow \infty$ ). The peak of  $\Gamma_1(1)-\Gamma_1(\infty)$  takes place at the Curie point, whereas the maximum of  $h(1)-h(\infty)$  is shifted into the ferromagnetic phase.

Within both the TCA and the MFA we have constructed the temperature-density phase diagrams of the model at different values of isotropic attraction between particles. At zero external field the obtained sequence of phase diagrams is (topologically) the same as in the Ising lattice gas; yet the field effect qualitatively differs. For example, in the plane-rotator LG without an isotropic attraction ( $v=0$ ) the field effect on the gas-liquid binodal is nonmonotonic: weak fields

lower the critical temperature (corresponding to the top of binodal), whereas strong fields slightly shift the binodal upward; in the Ising LG such behavior takes place only at sufficiently large  $v$ , at  $v=0$  the external field monotonically lowers the binodal. The variety of the field effects on the gas-liquid binodal can be qualitatively explained by the ‘‘bistendency’’ mechanism proposed in Ref. 22. Our results show that the lowering tendency decreases in the sequence: Ising, plane-rotator, Heisenberg fluids. In other words, the external field loses its ability to decrease the gas-liquid critical temperature when the number of possible spin orientations increases.

One can see that the lattice gas approach may be successfully used for description of complex fluids when continuous approaches lead to too complex calculations or do not give satisfactory results. For example, the TCA describes the effect of the nonmagnetic attraction on the Curie temperature; current liquid state theories<sup>21–24,28</sup> do not have such a capability.

## ACKNOWLEDGMENTS

R.S. thanks Tatiana Sokolovska for helpful discussions and valuable advice. The present calculations were carried out, on, among other machines, a cluster of DEC computers, belonging to the Sezione di Pavia of INFN (Istituto Nazionale di Fisica Nucleare); computer time was allocated by CINECA (Centro Interuniversitario Nord-Est di Calcolo Automatico, Casalecchio di Reno–Bologna), within INFN initiative on parallel computing; allocation of computer time by the Computer Center of Pavia University and CILEA (Consorzio Interuniversitario Lombardo per l’Elaborazione Automatica, Segrate–Milan) is also gratefully acknowledged. S.R. also acknowledges partial financial support by Ministero dell’Universita’ e della Ricerca Scientifica e Tecnologica (M.U.R.S.T.), through project Cofin MURST 97 CFSIB.

\*Electronic address: romano@pv.infn.it

<sup>†</sup>Author to whom correspondence should be addressed. Electronic address: ccc@icmp.lviv.ua

<sup>1</sup>H.-O. Carmesin, Phys. Lett. A **125**, 294 (1987).

<sup>2</sup>S. Romano, Nuovo Cimento Soc. Ital. Fis., B **100**, 447 (1987).

<sup>3</sup>S. Romano, Liq. Cryst. **6**, 457 (1989).

<sup>4</sup>S. Romano, Liq. Cryst. **12**, 641 (1992).

<sup>5</sup>Ya. G. Sinai, *Theory of Phase Transitions; Rigorous Results* (Pergamon Press, Oxford, 1982).

<sup>6</sup>H.-O. Georgii, *Gibbs Measures and Phase Transitions* (de Gruyter, Berlin, 1988).

<sup>7</sup>N. Angelescu and V. A. Zagrebnov, J. Phys. A **15**, L639 (1982).

<sup>8</sup>N. Angelescu, S. Romano, and V. A. Zagrebnov, Phys. Lett. A **200**, 433 (1995).

<sup>9</sup>V. A. Zagrebnov, Physica A **232**, 737 (1996).

<sup>10</sup>S. Romano and V. A. Zagrebnov, Physica A **253**, 483 (1998).

<sup>11</sup>L. Chayes, K. Kotecký, and S. B. Shlosman, Commun. Math. Phys. **189**, 631 (1997).

<sup>12</sup>R. O. Sokolovskii, Phys. Rev. B **61**, 36 (2000).

<sup>13</sup>T. Kawasaki, Prog. Theor. Phys. **58**, 1357 (1977).

<sup>14</sup>J. M. Sanchez and C. H. Lin, Phys. Rev. B **30**, 1448 (1984).

<sup>15</sup>F. Y. Wu, Rev. Mod. Phys. **54**, 235 (1982).

<sup>16</sup>M. W. Conner and C. Ebner, Phys. Rev. B **36**, 3683 (1987).

<sup>17</sup>J. Kahng and C. Ebner, Phys. Rev. B **40**, 11 269 (1989).

<sup>18</sup>M. Blume, V. J. Emery, and R. B. Griffiths, Phys. Rev. A **4**, 1071 (1971).

<sup>19</sup>D. Lawrie and S. Sarbach, in *Phase Transitions and Critical Phenomena*, edited by C. Domb and J. L. Lebowitz (Academic Press, London, 1984), Vol. 9, Chap. 1, pp. 2–163.

<sup>20</sup>T. E. Burns and J. R. Dennison, Surf. Sci. **395**, 46 (1998).

<sup>21</sup>F. Schinagl, H. Iro, and R. Folk, Eur. Phys. J. B **8**, 113 (1999).

<sup>22</sup>T. G. Sokolovska and R. O. Sokolovskii, Phys. Rev. E **59**, 3819 (1999).

<sup>23</sup>H. Zhang and M. Widom, Phys. Rev. E **49**, R3591 (1994).

<sup>24</sup>B. Groh and S. Dietrich, Phys. Rev. Lett. **72**, 2422 (1994).

<sup>25</sup>H.-O. Georgii and V. A. Zagrebnov, J. Stat. Phys. **93**, 79 (1998).

<sup>26</sup>Recently developed integral equation theories and MC simulations (see Refs. 22,27, and references therein) predict that in the Heisenberg fluid near the top of the gas-liquid binodal both the gaseous and liquid phases can be ferromagnetic, which was never reported for Ising fluids.

<sup>27</sup>T. G. Sokolovska, Physica A **253**, 459 (1998).

<sup>28</sup>N. B. Wilding, F. Schmid, and P. Nielaba, cond-mat/9801265 (unpublished).

- <sup>29</sup>B. Ja. Balagurov, V. G. Vaks, and R. O. Zajtsev, *Fiz. Tverd. Tela* (Leningrad) **16**, 2302 (1974) [*Sov. Phys. Solid State* **16**, 1498 (1974)].
- <sup>30</sup>V. G. Vaks and N. Ye. Zein, *Zh. Éksp. Teor. Fiz.* **67**, 1082 (1974) [*Sov. Phys. JETP* **40**, 537 (1974)].
- <sup>31</sup>R. R. Levitskii, S. I. Sorokov, and R. O. Sokolovskii, *Acta Phys. Pol. A* **92**, 383 (1997).
- <sup>32</sup>D. Peña Lara and J. A. Plascak, *Int. J. Mod. Phys. B* **12**, 2045 (1998).
- <sup>33</sup>J. Lebowitz and O. Penrose, *J. Math. Phys.* **7**, 1016 (1966).
- <sup>34</sup>S. Romano, *Int. J. Mod. Phys. B* **13**, 191 (1999).
- <sup>35</sup>Z. W. Salsburg, J. D. Jacobson, W. Fickett, and W. W. Wood, *J. Chem. Phys.* **30**, 65 (1959).
- <sup>36</sup>L. D. Fosdick, *Phys. Rev.* **116**, 565 (1959).
- <sup>37</sup>L. Guttman, *J. Chem. Phys.* **34**, 1024 (1961).
- <sup>38</sup>P. A. Flinn and G. M. McManus, *Phys. Rev.* **124**, 54 (1961).
- <sup>39</sup>D. A. Chesnut and Z. W. Salsburg, *J. Chem. Phys.* **38**, 2861 (1963).
- <sup>40</sup>D. A. Chesnut, *J. Chem. Phys.* **39**, 2081 (1963).
- <sup>41</sup>W. Matthes, *J. Comput. Phys.* **4**, 431 (1969).
- <sup>42</sup>G. E. Norman and V. S. Filinov, *High Press. Res.* **7**, 216 (1969).
- <sup>43</sup>D. J. Adams, *Mol. Phys.* **28**, 1241 (1974); **29**, 307 (1975).
- <sup>44</sup>L. A. Rowley, D. Nicholson, and N. G. Parsonage, *J. Comput. Phys.* **17**, 401 (1975).
- <sup>45</sup>J. Yao, R. A. Greenkorn, and K. C. Chao, *Mol. Phys.* **46**, 587 (1982).
- <sup>46</sup>A. B. Harris, O. G. Mouritsen, and A. J. Berlinsky, *Can. J. Phys.* **62**, 915 (1984).
- <sup>47</sup>*Monte Carlo Methods in Statistical Physics*, 1st ed., edited by K. Binder (Springer, Berlin, 1979); *Applications of the Monte Carlo Methods in Statistical Physics*, 2nd ed., edited by K. Binder (Springer, Berlin, 1987).
- <sup>48</sup>*Simulation of Liquids and Solids: Molecular Dynamics and Monte Carlo Methods in Statistical Mechanics*, a collection of reprints edited by G. Ciccotti, D. Frenkel, and I. R. McDonald (North-Holland, Amsterdam, 1987).
- <sup>49</sup>M. P. Allen and D. J. Tildesley, *Computer Simulation of Liquids* (Oxford University Press, Oxford, UK, 1989).
- <sup>50</sup>T. Gruhn and M. Schoen, *Phys. Rev. E* **55**, 2861 (1997); *Mol. Phys.* **93**, 681 (1998); *J. Chem. Phys.* **108**, 9124 (1998); *Thin Solid Films* **330**, 46 (1998).
- <sup>51</sup>J. M. Polson and E. E. Burnell, *Chem. Phys. Lett.* **281**, 207 (1997).
- <sup>52</sup>J. F. Fernández and T. S. J. Streit, *Phys. Rev. B* **25**, 6910 (1982).
- <sup>53</sup>R. Gupta, J. De Lapp, G. G. Batrouni, G. C. Fox, C. F. Baillie, and J. Apostolakis, *Phys. Rev. Lett.* **61**, 1996 (1988); R. Gupta and C. F. Baillie, *Phys. Rev. B* **45**, 2883 (1992).
- <sup>54</sup>Y.-H. Li and S. Teitel, *Phys. Rev. B* **40**, 9122 (1989).
- <sup>55</sup>Y. Kadana and J. Mori, *Phys. Lett. A* **190**, 323 (1994).
- <sup>56</sup>K. Kawasaki, in *Phase Transitions and Critical Phenomena*, edited by C. Domb and M. S. Green (Academic Press, London, 1972), Vol. 2, Chap. 11, pp. 443–501.
- <sup>57</sup>T. L. Hill, *Statistical Mechanics: Principles and Selected Applications* (McGraw-Hill, New York, 1956).
- <sup>58</sup>B. Diu, C. Guthman, D. Lederer, and B. Roulet, *Éléments de Physique Statistique* (Hermann, Paris, 1989).
- <sup>59</sup>Th. T. A. Paauw, A. Compagner, and D. Bedaux, *Physica A* **79**, 1 (1975).
- <sup>60</sup>P. Peczak, A. M. Ferrenberg, and D. P. Landau, *Phys. Rev. B* **43**, 6087 (1991).
- <sup>61</sup>C. Zannoni, in *The Molecular Physics of Liquid Crystals*, edited by G. R. Luckhurst and G. W. Gray (Academic Press, London, 1979), Chap. 3, pp. 51–84.
- <sup>62</sup>C. Zannoni, in *The Molecular Physics of Liquid Crystals*, edited by G. R. Luckhurst and G. W. Gray (Ref. 61), Chap. 9, pp. 191–220.
- <sup>63</sup>S. Romano, *Europhys. Lett.* **2**, 431 (1987); *Nuovo Cimento D* **9**, 409 (1987).
- <sup>64</sup>E. T. Jaynes, *Phys. Rev.* **106**, 620 (1957); **108**, 171 (1957).
- <sup>65</sup>*The Maximum Entropy Formalism*, edited by R. D. Levine and M. Tribus (M.I.T. Press, Cambridge, MA, 1979).
- <sup>66</sup>D. I. Bower, *J. Polym. Sci., Polym. Phys. Ed.* **19**, 93 (1981).